Interface Engineering of Ru/RuO_2 Heterostructures on Carbon Nanotubes for Efficient and Stable Acidic Oxygen Evolution

Dazhou Kuang[a,b], Sheng Yao[a,b], Yang Yang*[a], Fangcai Zheng*[a,b], Hui Wang*[a,b]

[a] Hefei National Research Centre for Physical Sciences at the Microscale, Uuniversity of Science and Technology of China, Hefei, Anhui, 230026, P.R. China.

[b] High Magnetic Field Laboratory, Hefei Institutes of Physical. Science, Chinese Academy of Sciences, Hefei 230031, Anhui/P. R. China

1.Experimental Section

1.1 Chemical Reagents.

All reagents are of analytical grade and ready for use without further purification. Nitrogen-doped carbon nanotubes, benzene-1,3,5-benzenetricarboxylic acid ($C_9H_6O_6$), and ethanol (C_2H_5OH) were procured from Shanghai Aladdin Company Limited. Concentrated sulfuric acid (H_2SO_4) was obtained from Sinopharm Chemical Reagent limited corporation. Anhydrous ruthenium trichloride ($RuCl_3$) was procured from J&K Scientific Ltd. The deionized (DI) water used throughout all experiments was purified through a Millipore system.

1.2 Material synthesis

A quantity of 5 mg of nitrogen-doped carbon nanotubes was placed into a mixture of 10 mL of water and 10 mL of ethanol. The mixture was then stirred for a period of one hour in order to create a homogeneous dispersion. Following this, 28.2 mg of $RuCl_3$ was added and the mixture was stirred for a further hour. Then, 66.8 mg of benzene-1,3,5-benzenetricarboxylic acid was added and the mixture was stirred for a period of 4-6 hours. In conclusion, the substance was loaded into centrifuge tubes and subsequently introduced into a freeze dryer. The precursor was obtained following the drying process. The precursor was heated to 600 °C at a heating rate of 10 °C/min under an N_2 atmosphere and held for two hours to obtain black Ru@CNT. This was then oxidized at low temperatures to obtain Ru/RuO_2@CNT-250, Ru/RuO_2@CNT-300, and Ru/RuO_2@CNT-350 by oxidizing the precursor at low temperatures under an air atmosphere at 250 °C, 300 °C, and 350 °C, respectively. The precursor was subjected to oxidation at elevated temperatures, resulting in the formation of RuO_2@CNT.

1.3 Characterization.

Powder XRD pattern was performed using a Japan Rigaku D/Max-γA X-ray diffractometer equipped with Cu−Kα radiation. Morphologies and size of all as-synthesized samples were systematically characterized through scanning electron microscopy (SEM, Regulus 8230). Transmission electron microscopy (TEM) images were taken on a TEM (JEOL JEM-F200) and transmission electron microscopy (TEM,

Hitachi H-7650) equipped with Super-X energy dispersive X-ray (EDX) spectroscopy. X-ray photoelectron spectroscopy (XPS) analysis was carried out on an X-ray photoelectron spectrometer (ThermoFisher Escalab 250Xi) using Al-Kα radiation. Raman scattering measurement was performed using a Horiba Jobin YvonT64000 Micro-Raman instrument with a torus 532 laser (λ=532 nm) as an excitation source.

1. 4 Calculation details:

We perform DFT calculations using the Vienna Ab Initio Simulation Package (VASP), the generalized gradient approximation (GGA) of Perdew−Becke−Ernzerhof (PBE) is used for the exchange-correlation functional. The cut-off energy for plane waves is 400 eV, providing a convergence of 10^{-5} eV in total energy and 0.02 eV/Å in Hellmann Feynman force on each atom. The k-point mesh of 3 × 3 × 1 and 9 × 9 × 3 were used to represent the Brillouin zone for structure optimization and density of states (DOS) calculation, respectively. As for OER, the free energies of the intermediates at 298.15 K were obtained using $\triangle G=\triangle E+\triangle ZPE-T\triangle S+eU$ according to previous work, where ΔE is the binding energy of adsorption species HO*, O* and HOO*, ΔZPE, ΔS and U are the zero point energy changes, entropy changes and applied potentials, respectively.

1.5 Electrochemical measurements.

All electrochemical experiments were conducted at ambient temperature using an electrochemical workstation (CHI 760E) in a three-electrode system. The cell comprised a glassy carbon working electrode (GC electrode, diameter 3 mm, catalyst loading ~0.510 mg cm^{-2}), a $Hg/HgSO_4$ (saturated K_2SO_4 solution) reference electrode and a platinum mesh electrode. In this study, all potentials are expressed in relation to the transformed reversible hydrogen electrode (RHE) (ERHE= E_{Hg/Hg_2SO_4}+0.656+0.0592 pH). The overpotential (η) of the oxygen evolution reaction (OER) is defined as ERHE-1.23 V. The working electrodes were prepared by applying 5 μL of catalyst ink to glassy carbon (GC) and drying at room temperature. The electrode was meticulously polished by applying 0.05 μm Al_2O_3 powder prior to its utilization, and the electrode was

thoroughly rinsed with deionized water and ethanol. A quantity of 2 mg of catalyst was dispersed in a solution comprising 190 μL of ethanol, 65 μL of deionized water and 25 μL of Nafion solution (Sigma Aldrich, 5 wt %). The dispersion was then subjected to ultrasonication for a minimum of 30 minutes, with the objective of forming a homogeneous catalyst ink. The OER data were collected in O_2-saturated 0.5 M H_2SO_4. LSV curves were acquired at a scan rate of 5 mV/s. Cyclic voltammetry (CV) was conducted within the potential range of 1.05 to 1.50 V vs. RHE at a scan rate of 100 mV/s for a total of 2500 cycles, with the objective of assessing the long-term cycling stability. Electrochemical impedance spectroscopy (EIS) measurements were conducted for OER within the frequency range of 0.01 Hz to 10^6 Hz.

Under conditions of open circuit voltage, the electrochemically active surface areas (ECSAs) of the catalysts were estimated by electrochemical double layer capacitance (C_{dl}). The C_{dl} was measured from the double-layer charging curves using cyclic voltammetry (CV) with scan rates ranging from 20 to 100 mV s^{-1} and OERs ranging from 1.05 to 1.15 V vs. RHE, corresponding to non-Faraday capacitance current densities of 1.1 V vs. RHE, and $\Delta j/2$) at RHE as a linear curve with scan rate, with a slope of C_{dl}. ECSA was calculated from the double-layer capacitance according to ECSA = C_{dl}/CS, where CS is the specific capacitance of the sample. The general specific capacitance value of 0.035 mF cm^{-2} utilized in this study is based on values commonly reported in the extant literature

1.6 In-situ Fourier transform infrared spectroscopy measurements:

The in-situ Fourier transform infrared spectroscopy (FT-IR) measurements were carried out using the Nicolet iS50 FT-IR spectrometer to investigate the potential dependence of intermediates and determine the reaction mechanism of OER. In situ infrared reflectance spectroscopy (IRAS) measurements were performed in a 0.5 M H_2SO_4 solution using a three-electrode system. The working electrode was prepared by loading the catalyst onto a glassy carbon electrode. An Ag/AgCl electrode (in a saturated KCl solution) and a platinum wire served as the reference and counter electrodes, respectively. Prior to data acquisition, the working electrode was pressed against a CaF_2 infrared window in order to obtain a thin electrolyte layer. Subsequently,

sample and reference spectra were acquired at corresponding electrode potentials. The FT-IR spectra were recorded over the range of 1000 to 4000 cm^{-1} at various potentials and under different conditions of polarization. It is important to note that each measurement was of a duration of at least 2 minutes in order to ensure stable current.

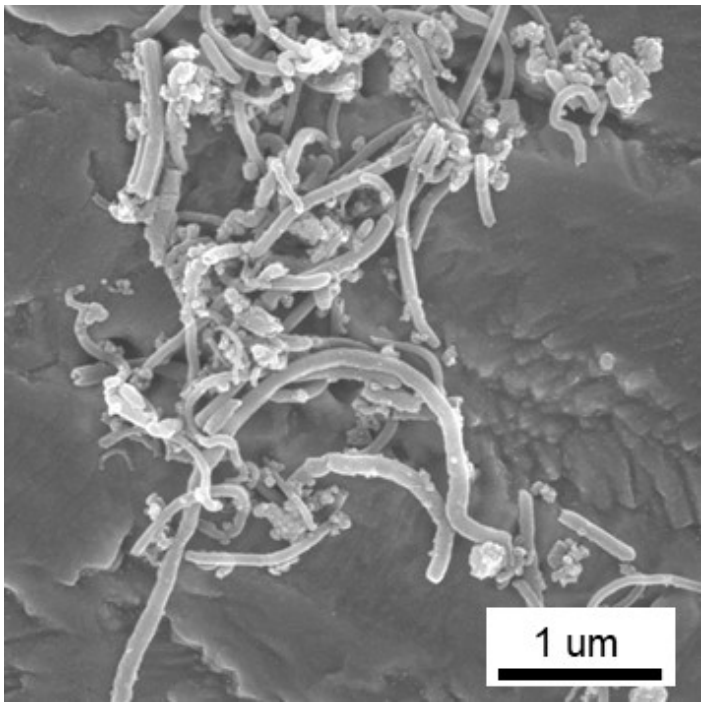

Figure S1. SEM image of Ru/RuO_2@CNT-300.

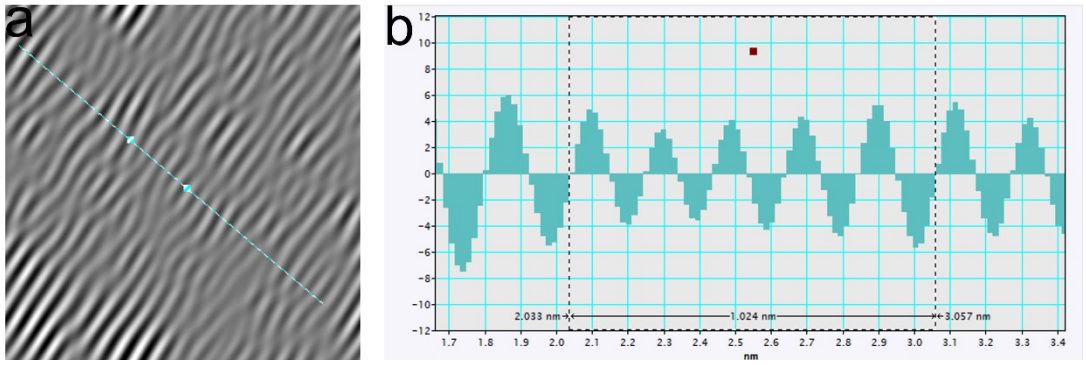

Figure S2. (a) HAADF-TEM image of the Ru/RuO_2@CNT-300 catalyst. (b) Ru/RuO_2@CNT-300 Ru(101) crystallographic spacing measurements of crystal faces.

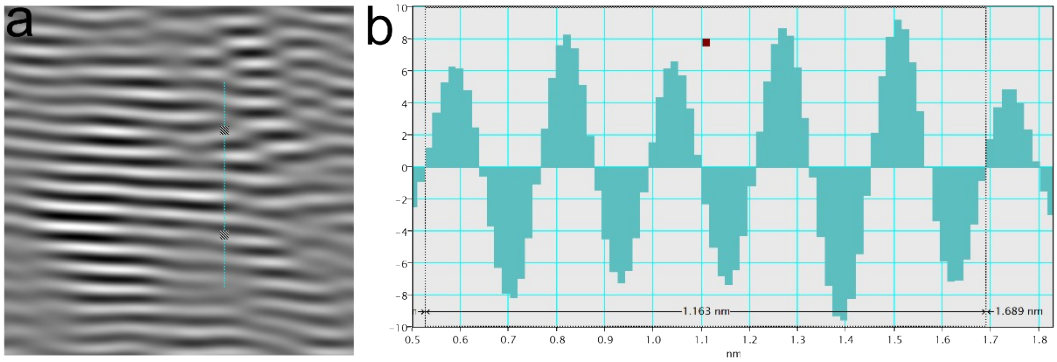

Figure S3. (a) HAADF-TEM image of the Ru/RuO_2@CNT-300 catalyst. (b) Ru/RuO_2@CNT-300 Ru(100) crystallographic spacing measurements of crystal faces.

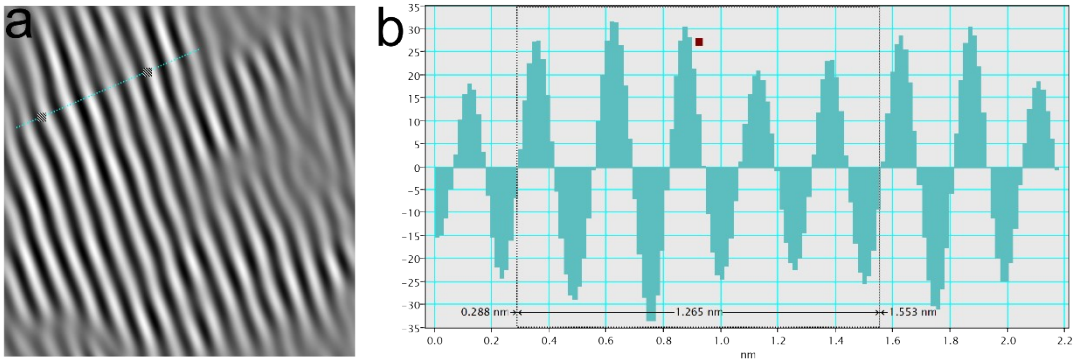

Figure S4. (a) HAADF-TEM image of the Ru/RuO_2@CNT-300 catalyst. (b) Ru/RuO_2@CNT-300 RuO_2(101) crystallographic spacing measurements of crystal faces.

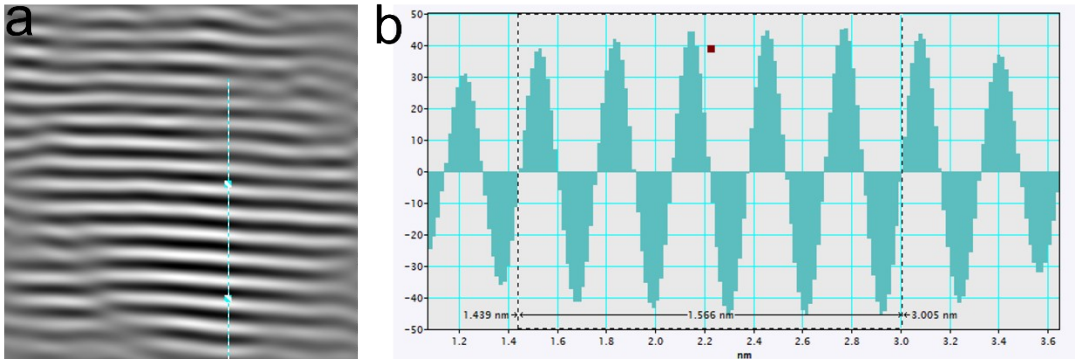

Figure S5. (a) HAADF-TEM image of the Ru/RuO_2@CNT-300 catalyst. (b) Ru/RuO_2@CNT-300 RuO_2(110) crystallographic spacing measurements of crystal faces.

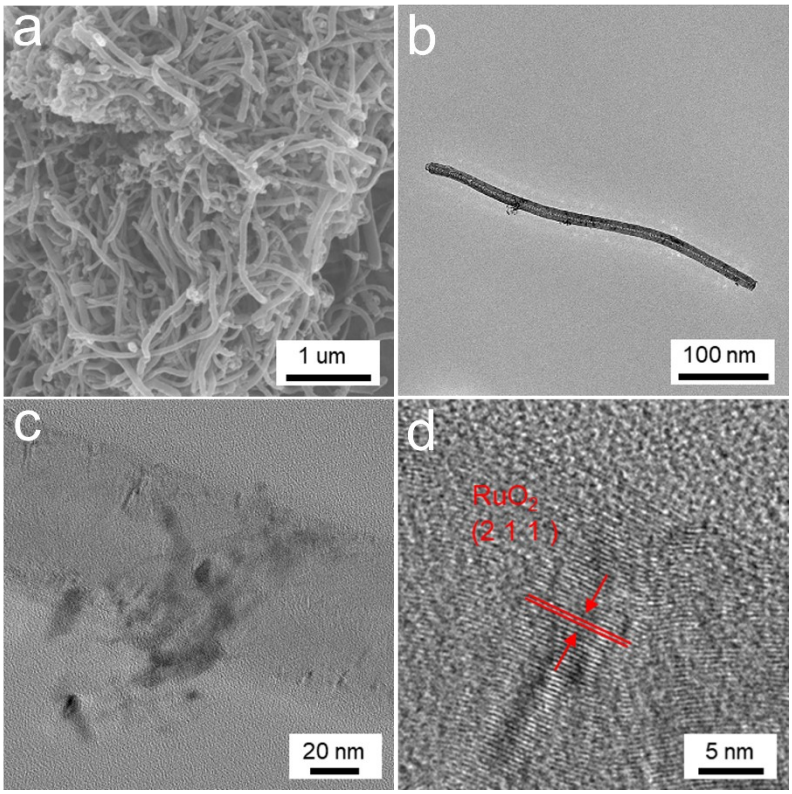

Figure S6. (a) SEM and (b,c,d) TEM images of RuO_2@CNT

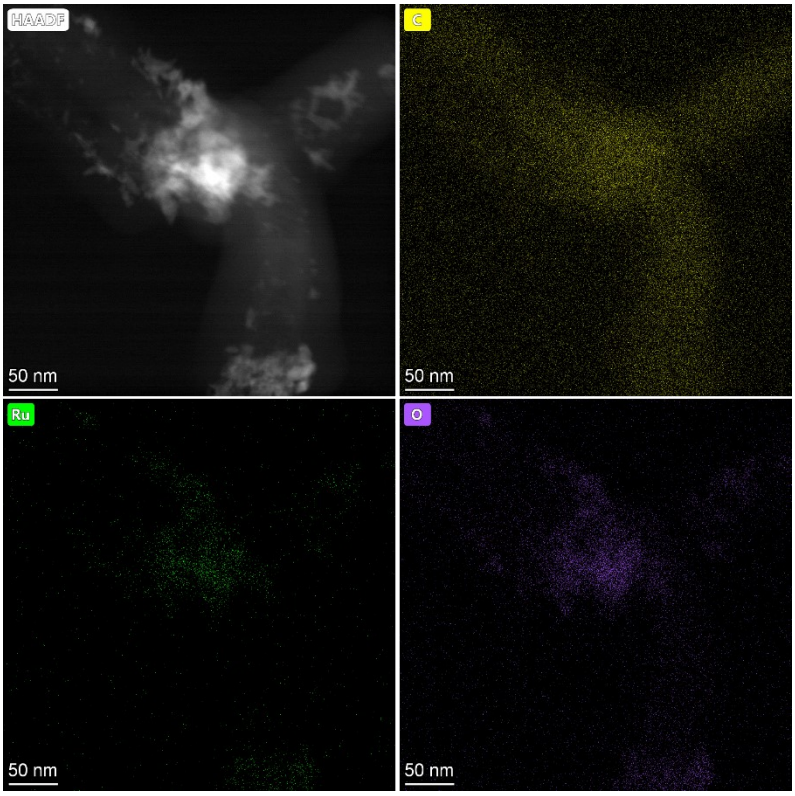

Figure S7. EDS mappings of RuO_2@CNT

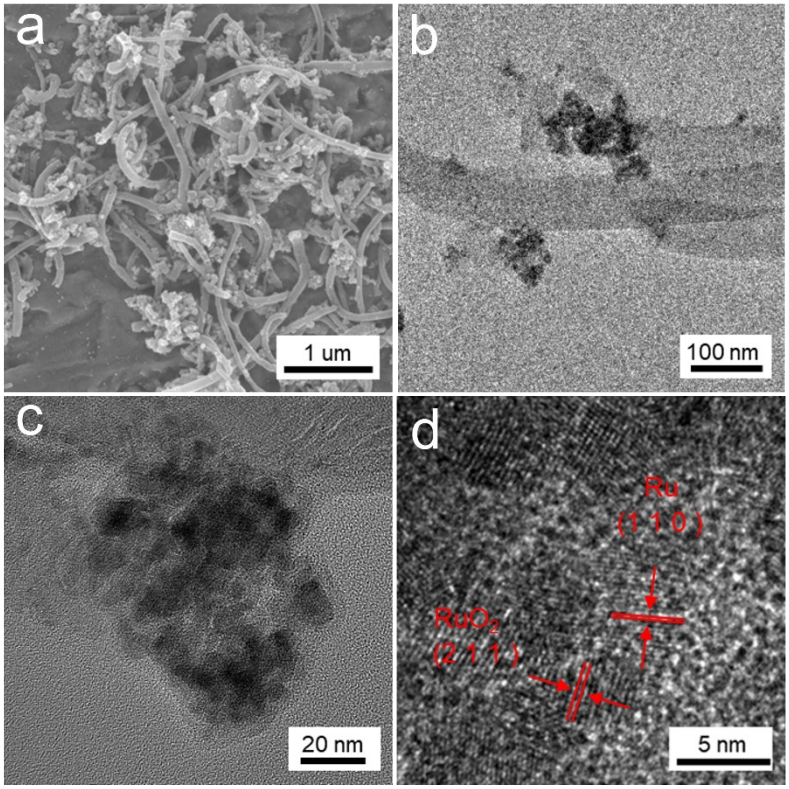

Figure S8. (a) SEM and (b-d) TEM images of Ru/RuO_2@CNT-350

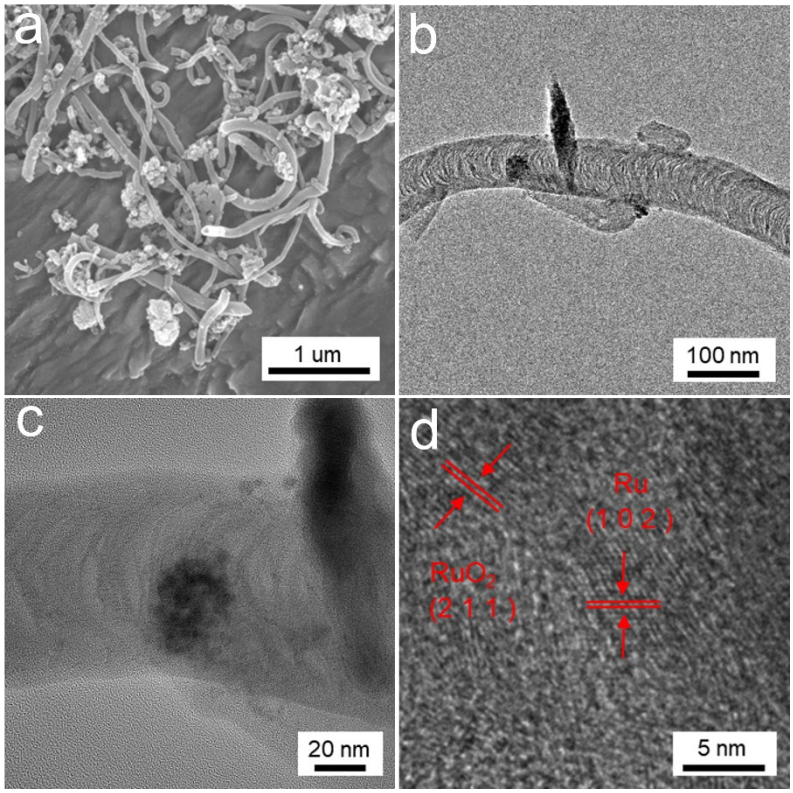

Figure S9. (a) SEM and (b-d) TEM images of Ru/RuO_2@CNT-250

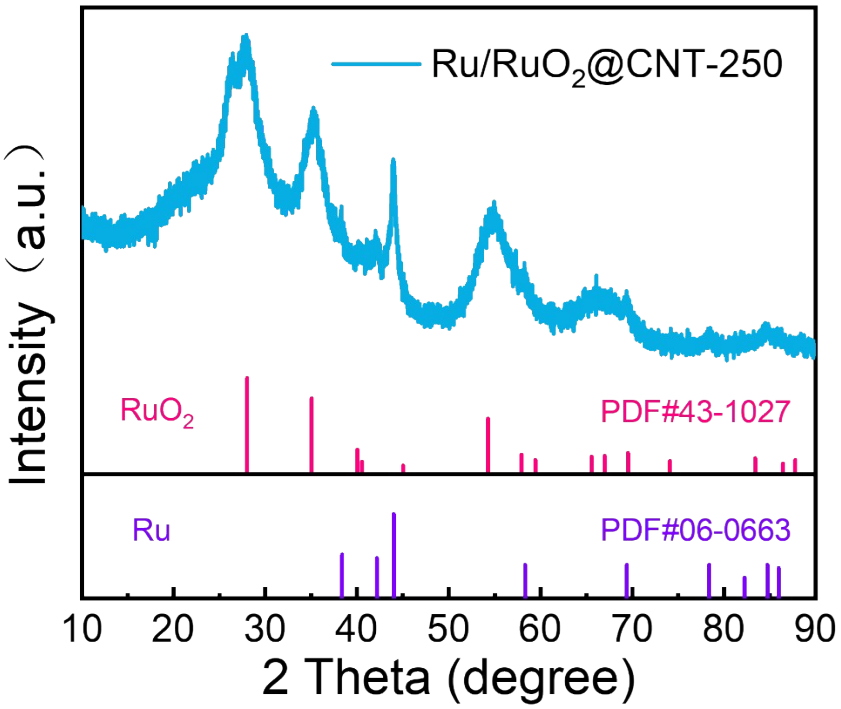

Figure S10. XRD pattern of Ru/RuO_2@CNT-250.

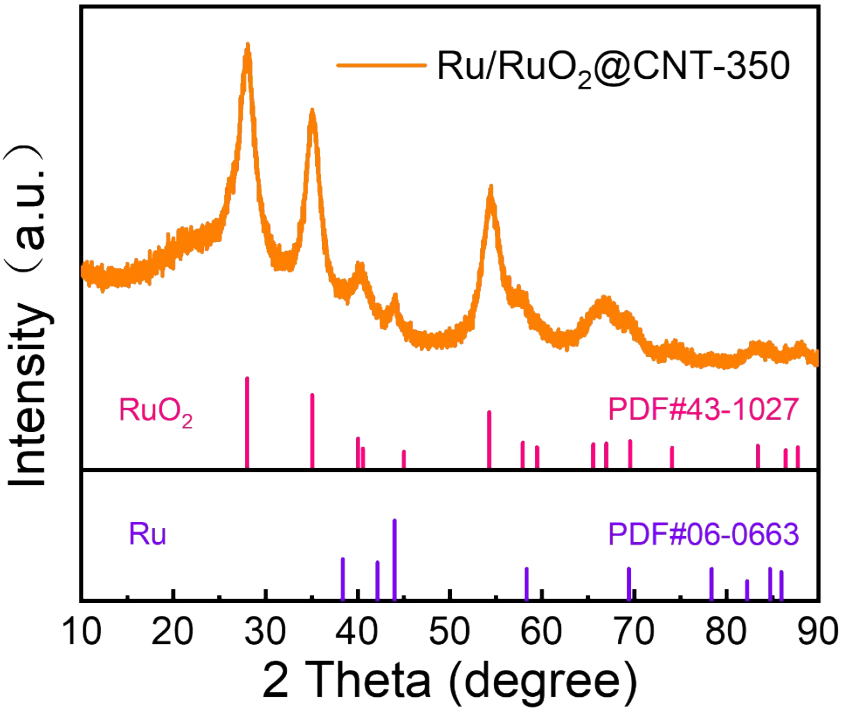

Figure S11. XRD pattern of Ru/RuO_2@CNT-350.

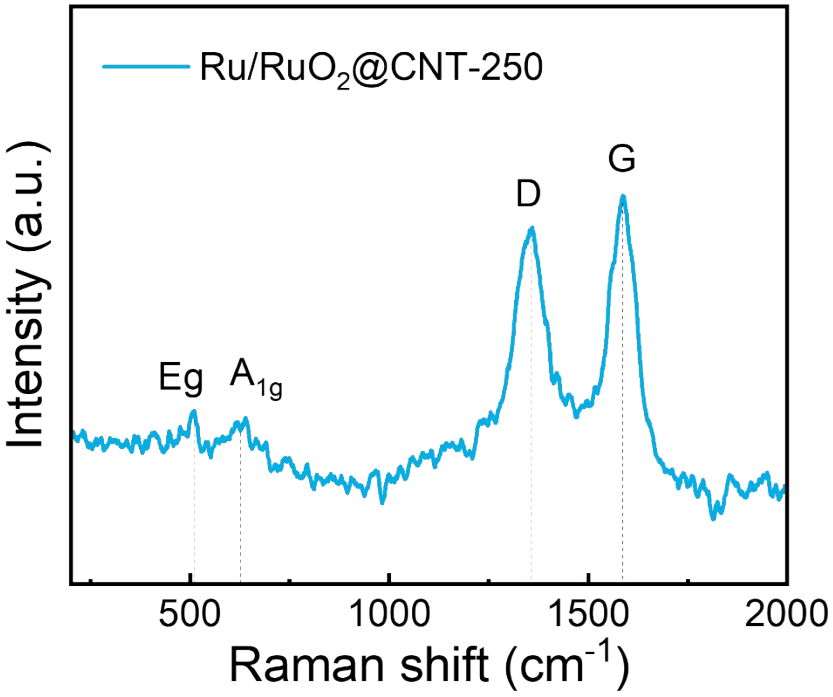

Figure S12. Raman spectrum of Ru/RuO_2@CNT-250.

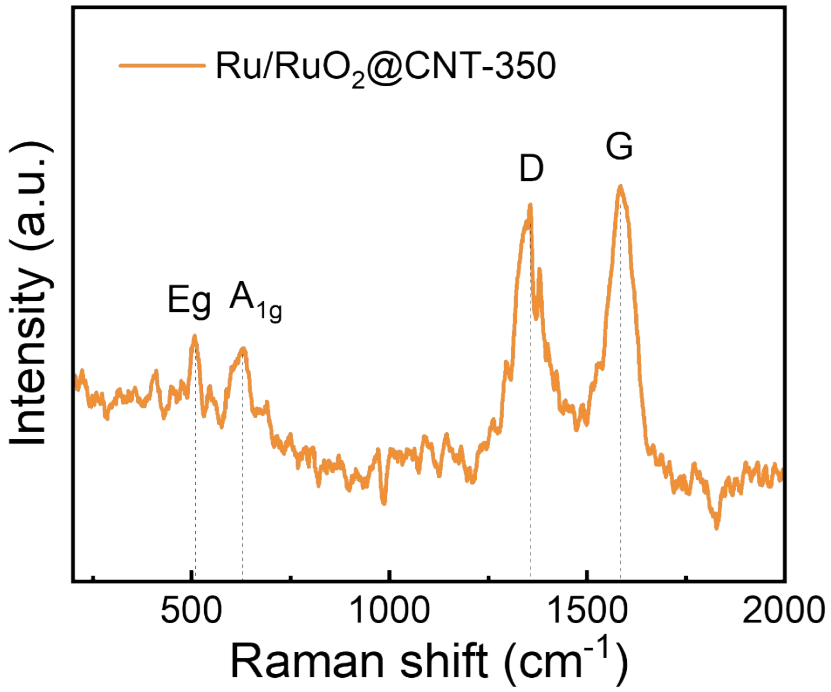

Figure S13. Raman spectrum of Ru/RuO_2@CNT-350.

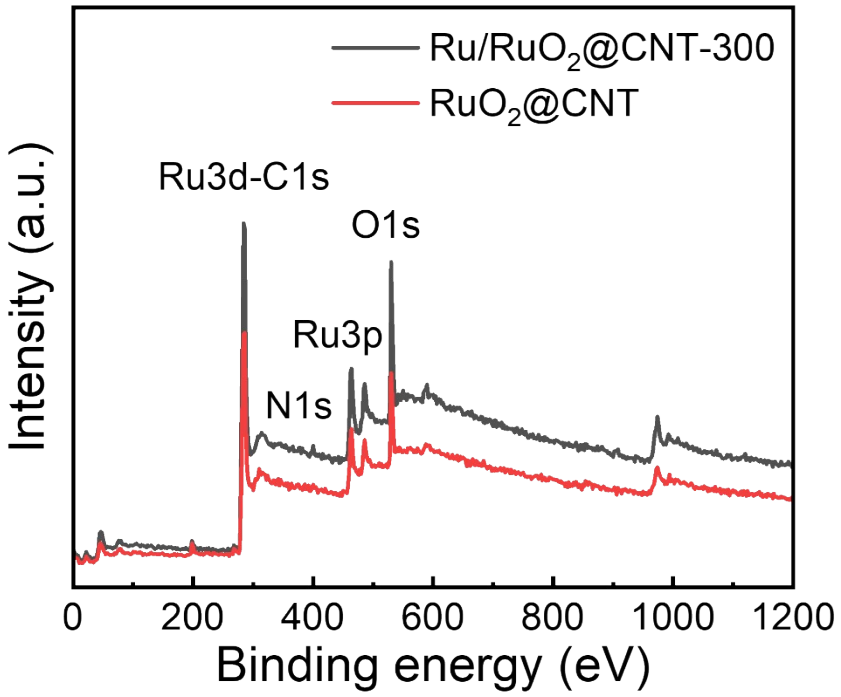

Figure S14. XPS survey spectra of Ru/RuO_2@CNT-300 and RuO_2@CNT.

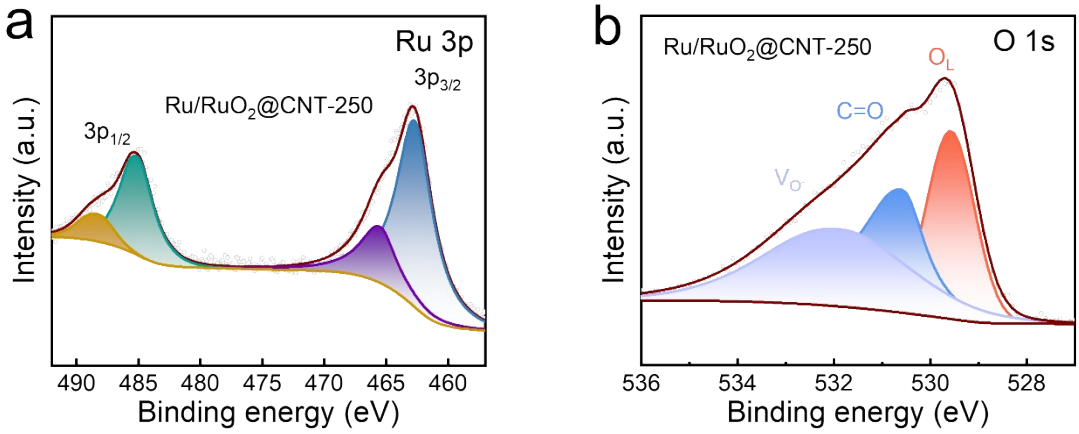

Figure S15. High-resolution spectra of (a) Ru 3p and (b) O 1s for Ru/RuO_2@CNT-250.

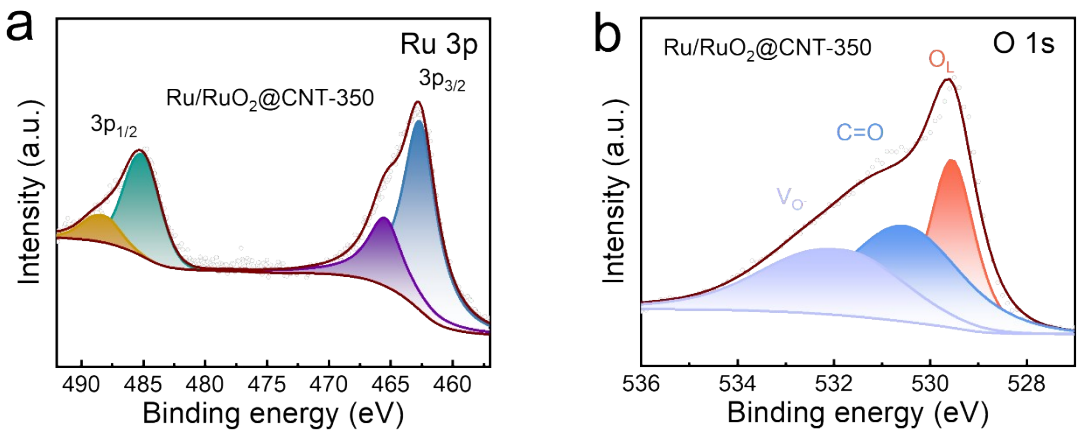

Figure S16. High-resolution spectra of (a) Ru 3p and (b) O 1s for Ru/RuO_2@CNT-350.

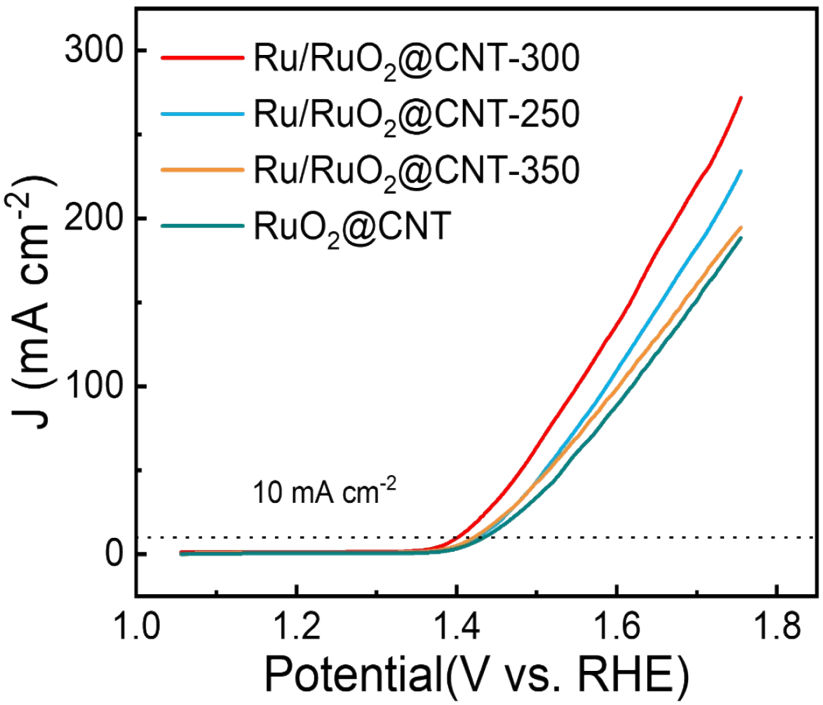

Figure S17. LSV Diagram Without IR Compensation.

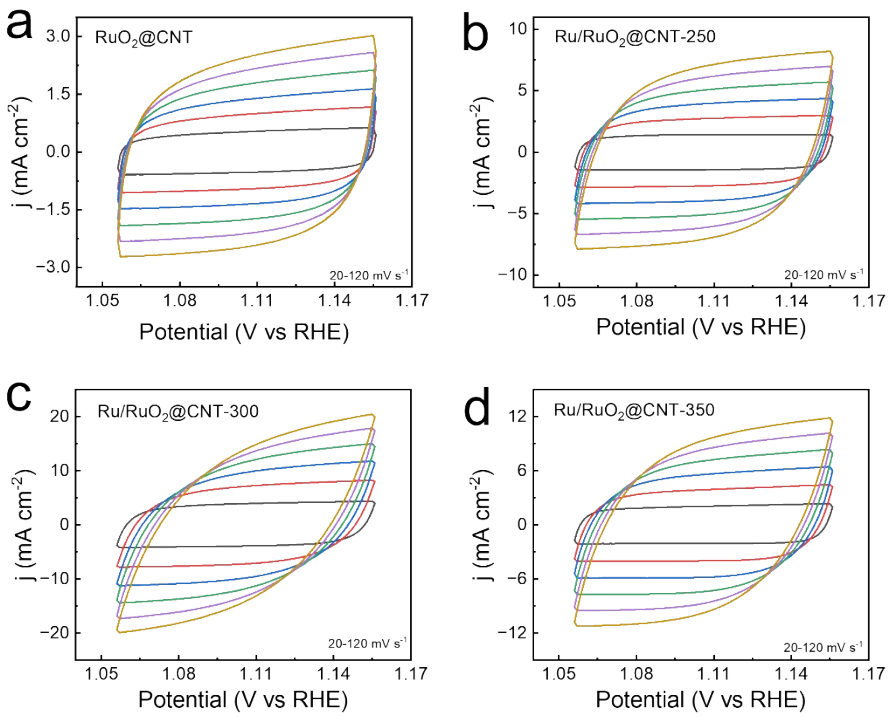

Figure S18. The OER CV curves of (a) RuO_2@CNT, (b) Ru/RuO_2@CNT-250, (c) Ru/RuO_2@CNT-300 and (d) Ru/RuO_2@CNT-350 with different scan rates in 0.5 M H_2SO_4.

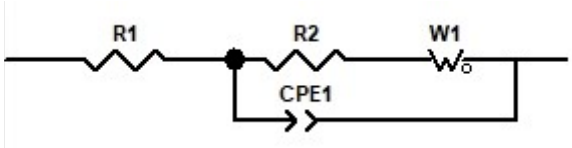

Figure S19. Circuit diagram for EIS fitting.

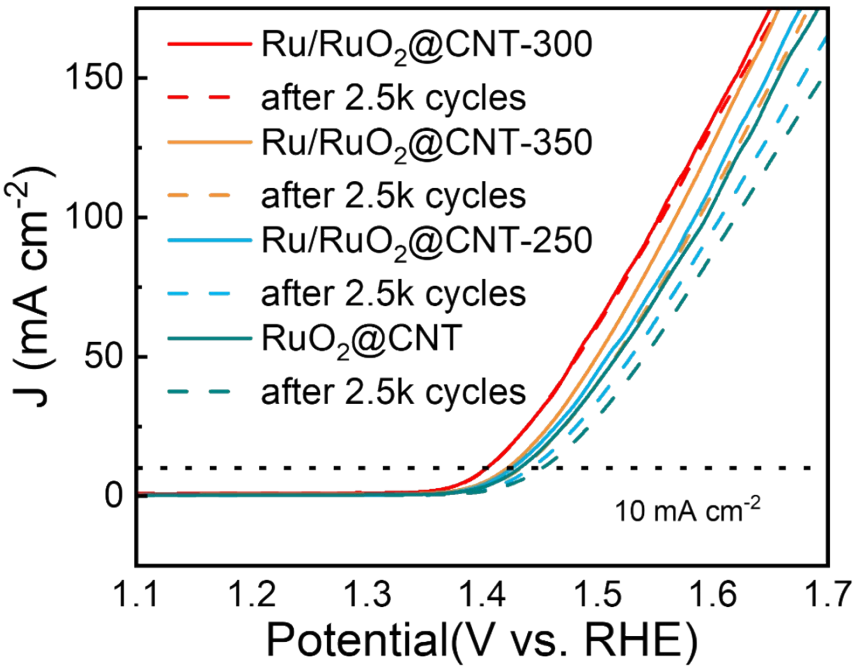

Figure S20. LSV curves before and after 2500 CV tests at 100 mV s^{-1}.

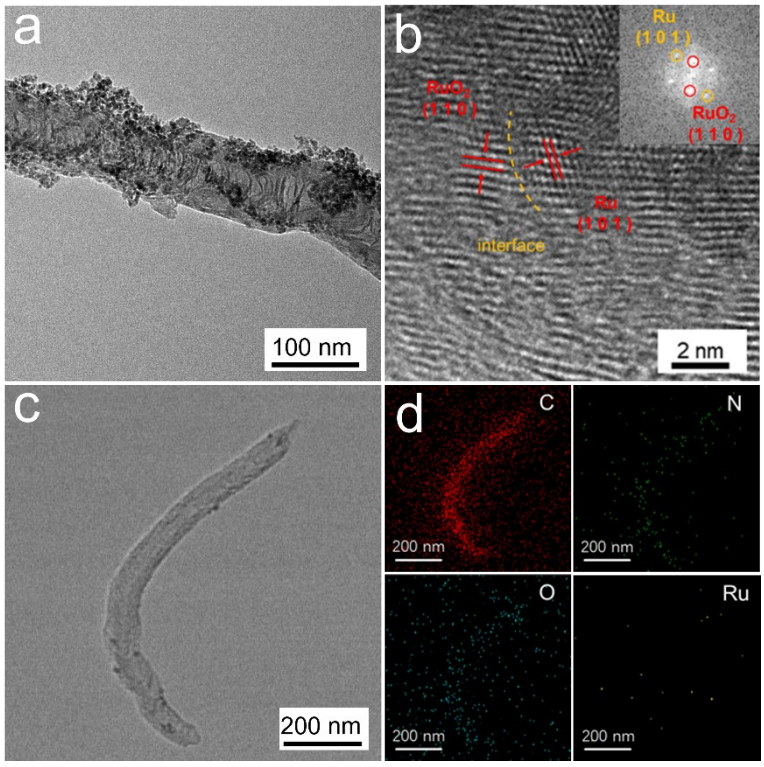

Figure S21. (a,b) TEM images of Ru/RuO_2@CNT-300 during OER test in 0.5 M H_2SO_4. (c,d) EDS mappings of Ru/RuO_2@CNT-300 during OER test in 0.5 M H_2SO_4.

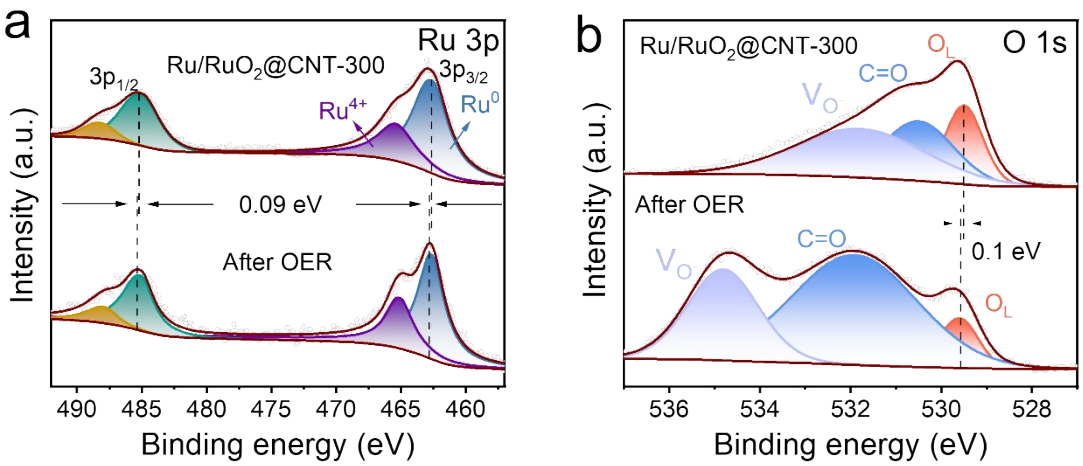

Figure S22. (a) Ru 3p, (b) O 1s XPS spectra of Ru/RuO_2@CNT-300 before and after OER test.

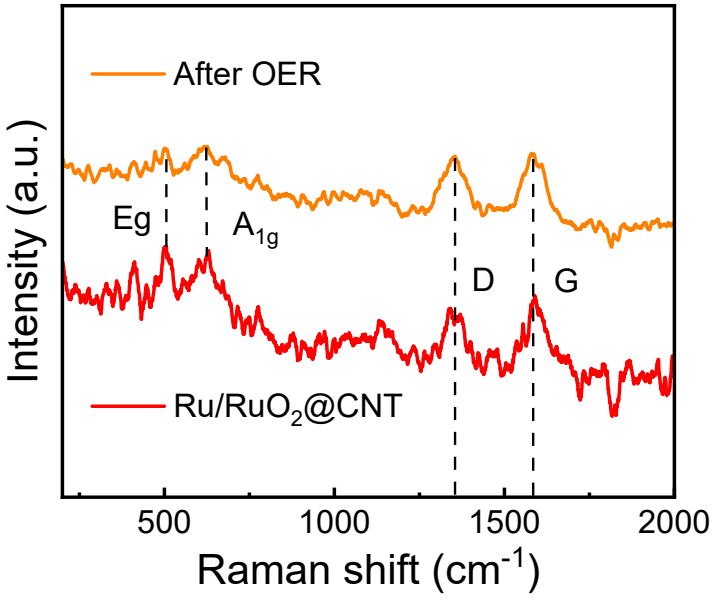

Figure S23: Raman spectra of Ru/RuO_2@CNT-300 before and after oxygen evolution reaction (OER) testing.

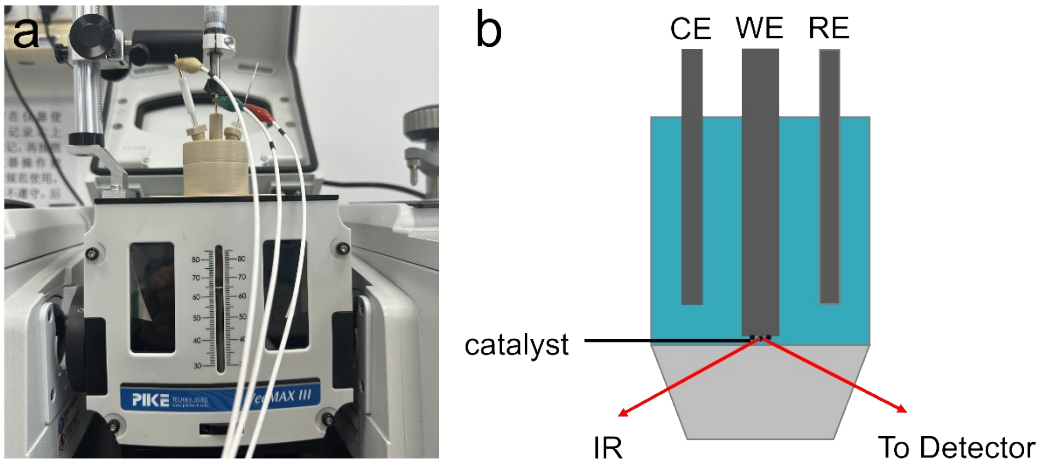

Figure S24. (a) Photograph and (b) schematic illustration of the setup for in-situ IRAS measurements.

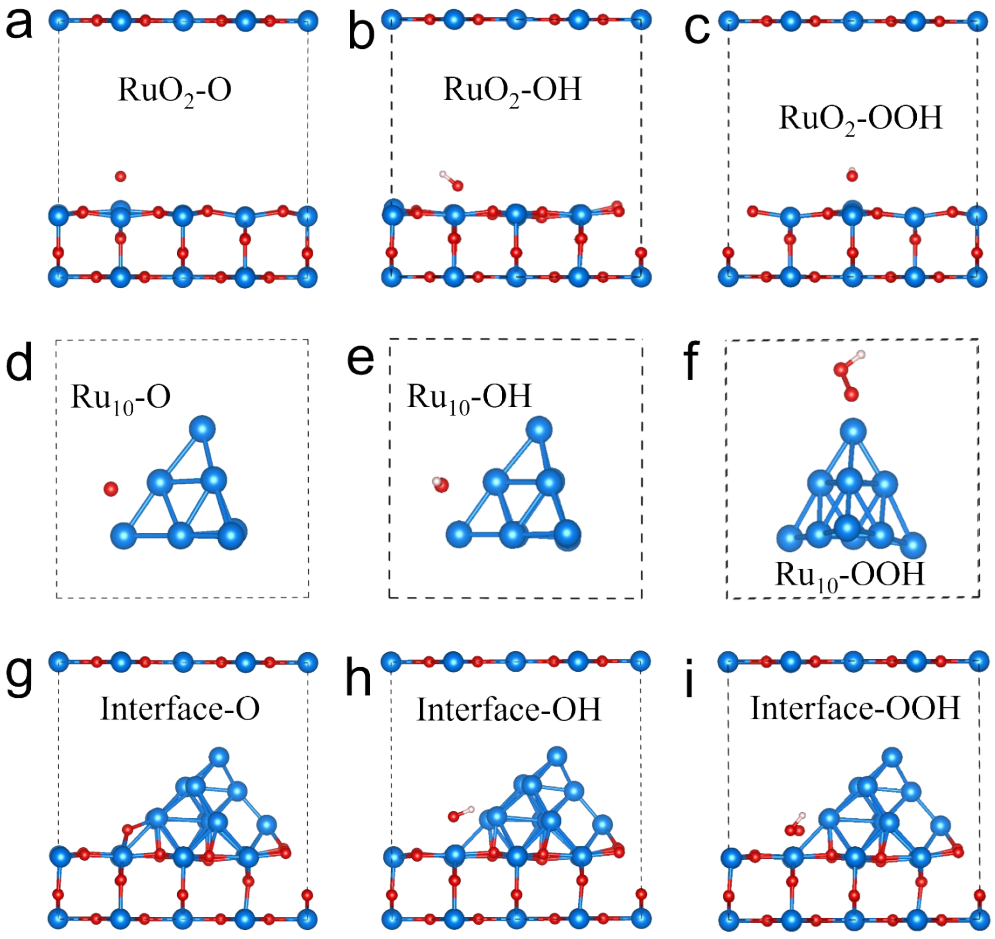

Figure S25. (a-c) RuO_2 (110) surface, (d-f) Ru cluster (Ru10), (g-i) Ru/RuO_2 adsorption model.

Table S1. OER performance on Ru/RuO_2@CNT-300 in comparison with the recently reported electrocatalysts in acidic and alkaline media.

Catalyst	Electrolyte	Overpotential @ 10 mA cm^{-2}	Stability @ 10 mA cm^{-2}	Reference
Ru/RuO_2@CNT-300	0.5 M H_2SO_4	169 mV	120 h	This work
IrO_x /WO_3	0.5 M H_2SO_4	260 mV	100 h	[1]
$Nd_{0.1}$RuOx/CC	0.5 M H_2SO_4	211 mV	50 h	[2]
Co-RuO_2 /TiO_2	0.5 M H_2SO_4	266 mV	50 h	[3]
RuO_2 /$(Co,Mn)_3O_4$	0.5 M H_2SO_4	270 mV	24 h	[4]
Cr_2O_3 /RuO_2	0.5 M H_2SO_4	220 mV	100 h	[5]
Co_3O_4 /NC-250	0.5 M H_2SO_4	225 mV	80 h	[6]
H/d-MnO_x-RuO_2	0.5 M H_2SO_4	178 mV	40 h	[7]
Ru/Se-RuO_2	0.5 M H_2SO_4	190 mV	24 h	[8]
a/c-RuO_2	0.1 M $HClO_4$	205 mV	60 h	[9]
$Nd_6Ir_2O_{13}$	0.1 M $HClO_4$	291 mV	19.5 h	[10]
$MgNiO_2$/rGO	1 M KOH	209 mV	50h	[11]

Table S2. ICP-AES results of prepared samples.

Samples	Ru (wt %)
Ru/RuO_2@CNT-300	2.25
After OER	2.24

Supplementary References

1. J. Xu, H. Jin, T. Lu, J. Li, Y. Liu, K. Davey, Y. Zheng, S.-Z. Qiao. *Sci. Adv.* **9**, eadh1718.
2. L. Li, G. Zhang, J. Xu, H. He, B. Wang, Z. Yang, S. Yang. *Adv. Funct. Mater.* 2023, **33**, 2213304.
3. L. Lu, Z. Xu, S. Wei, S. Zhao, X. Du, Y. Wang, L. Wu, G. Liu. *Chem. Eng. J.* 2024, **500**, 157107.
4. S. Niu, X.-P. Kong, S. Li , Y. Zhang, J. Wu, W. Zhao, P. Xu. *App. Catal. B: Environ.* 2021, **297**, 120442.
5. J. Zhao, N. Yao, W. Luo. *ChemistrySelect* 2025, **10**, e01065.
6. X. Yang, J. Cheng, H. Li, Y. Xu, W. Tu, J. Zhou. *Chem. Eng. J.* 2023, **465**, 142745.
7. Z. Wu, Y. Wang, D. Liu, B. Zhou, P. Yang, R. Liu, W. Xiao, T. Ma, J. Wang, L. Wang. *Adv. Funct. Mater.* 2023, **33**, 2307010.
8. K. Huang, C. Lin, G. Yu, P. Du, X. Xie, X. He, Z. Zheng, N. Sun, H. Tang, X. Li, M. Lei, H. Wu. *Adv. Funct. Mater.* 2023, **33**, 2211102.
9. L. Zhang, H. Jang, H. Liu, M.G. Kim, D. Yang, S. Liu, X. Liu, J. Cho. *Angew. Chem. Int. Ed.* 2021, **60**, 18821-18829.
10. L. Zhang, Y. Wang, Y. Wang, H. Liu, Q. Qin, X. Liu. *ACS Sustainable Chem. Eng.* 2022, **10**, 10658-10665.
11. K. Ashfaq , F.F. Alharbi , A. Kumar , M. Faizan , B. Kanabar , N. Beemkumar , P. Pradhan , T. Aggarwal , M.A. Al-Anber, A.D. Oza. *J Inorg Organoment P 2025.*